Progress Toward a Molecular Mechanism of Water Oxidation in Photosystem II

David J. Vinyard[1] and Gary W. Brudvig[2]

[1]Department of Biological Sciences, Louisiana State University, Baton Rouge, Louisiana 70803; email: dvinyard@lsu.edu

[2]Department of Chemistry, Yale University, New Haven, Connecticut 06520; email: gary.brudvig@yale.edu

Keywords

photosynthesis, solar fuels, oxygen evolution

Abstract

The active site of photosynthetic water oxidation is the oxygen-evolving complex (OEC) in the photosystem II (PSII) reaction center. The OEC is a Mn_4CaO_5 cluster embedded in the PSII protein matrix, and it cycles through redox intermediates known as S_i states ($i = 0$–4). Significant progress has been made in understanding the inorganic and physical chemistry of states S_0–S_3 through experiment and theory. The chemical steps from S_3 to S_0 are more poorly understood, however, because the identity of the substrate water molecules and the mechanism of O–O bond formation are not well established. In this review, we highlight both the consensuses and the remaining challenges of PSII research.

INTRODUCTION

In oxygenic photosynthesis, the photosystem II (PSII) reaction center uses visible light to extract electrons and protons from water. The O_2 produced in this reaction (Equation 1) is released to the environment, having provided an excellent electron sink for efficient respiration (1). The released electrons are used to reduce plastoquinone (PQ) to plastoquinol (PQH_2) (Equation 2). The PQH_2 produced and the protons pumped across the thylakoid membrane are used in the photosynthetic electron-transport chain to generate the nicotinamide adenine dinucleotide phosphate (NADPH) and adenosine triphosphate (ATP) needed for CO_2 fixation and general anabolism (1, 2).

$$2H_2O \rightarrow O_2 + 4e^- + 4H^+_{lumen}, \qquad\qquad 1.$$

$$2PQ + 4e^- + 4H^+_{stroma} \rightarrow 2PQH_2. \qquad\qquad 2.$$
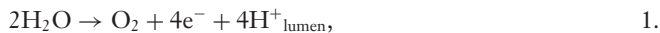
Charge separation in PSII occurs when the primary chlorophyll-a electron donor, P_{680}, absorbs a visible photon or receives an exciton from peripheral antenna pigments. The excited electron in P_{680}^* is efficiently and quickly transferred to pheophytin-a, which in turn transfers the electron to the primary PQ electron acceptor, Q_A. Q_A reduces the secondary PQ acceptor, Q_B, via a nonheme iron center. When Q_B has accepted two electrons (and two protons from the stroma) to form PQH_2, it diffuses out of the reaction center and into the thylakoid membrane–soluble PQ pool and is replaced by an oxidized PQ molecule (for a review, see 3). These electron-transfer steps from P_{680}^* to PQH_2 are collectively known as the acceptor side of PSII and determine the reaction center's turnover frequency (TOF) (see the sidebar titled How Fast Is PSII?).

This review focuses on the donor side of PSII, which includes the electron-transfer steps from water to P_{680}^+. Following charge separation, a redox-active tyrosine residue, Y_Z, reduces P_{680}^+ and oxidizes the oxygen-evolving complex (OEC). The OEC is a Mn_4CaO_5 cluster embedded in the PSII protein matrix near the lumenal surface (**Figure 1**) (4, 5). Oxidizing water requires that four electrons and four protons be stripped from two molecules of water (Equation 1). Therefore, each
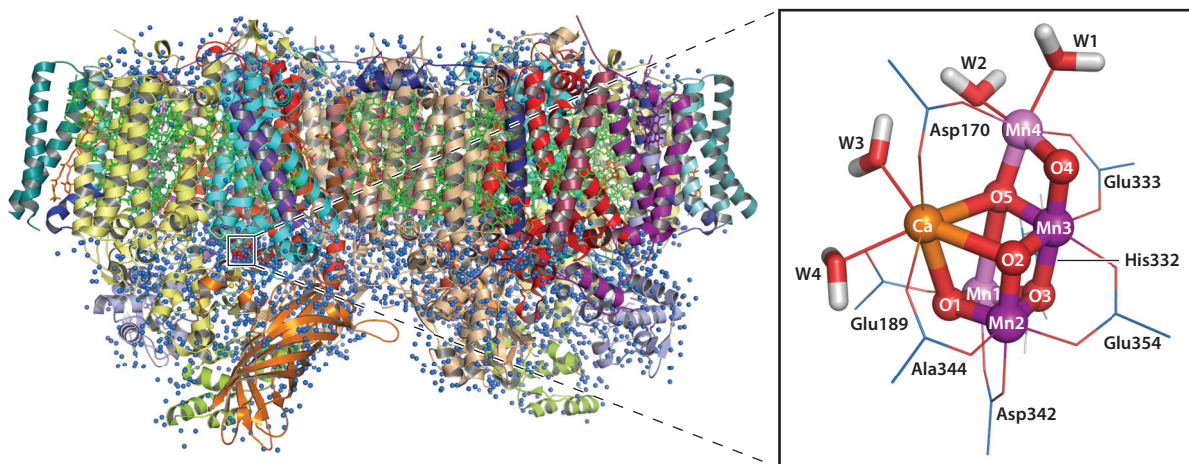
Figure 1

The oxygen-evolving complex (OEC) in its dark resting state (S_1) is a $Mn_4CaO_5(H_2O)_4$ inorganic cluster embedded in the photosystem II (PSII) reaction center near the lumenal surface. The X-ray crystal structure of the dimeric PSII complex has been solved to 1.9-Å resolution (4). Crystallographic waters are shown as blue spheres. (*Inset*) The quantum mechanics/molecular mechanics optimized structure of the OEC in the S_1 state. Figure generated in PyMOL from Protein Data Bank file 3WU2 and coordinates from Reference 8.

HOW FAST IS PSII?

By simply summing the rate constants of the individual S-state transitions, we see that the OEC can produce one molecule of O_2 from two molecules of H_2O with a half-time of approximately 1.4–2.0 ms (86–88). This rate corresponds to a turnover frequency (TOF) of 500–700 $O_2/(s \cdot PSII)$. However, the measured TOF of the OEC is only about 30 $O_2/(s \cdot PSII)$ (for a review, see 3). The fastest TOF reported in vitro is 67 $O_2/(s \cdot PSII)$ in PSII core complexes from *Thermosynechococcus elongatus* (89, 90), and the fastest TOF reported in vivo is 88 $O_2/(s \cdot PSII)$ from *Arthrospira maxima* (91). This discrepancy between the theoretical and measured rates of O_2 release indicates that OEC cycling does not include the rate-determining step for overall turnover of PSII. Instead, electron transfer on the acceptor side of PSII limits the kinetics of water oxidation. The half-time of electron transfer from Q_A^- to Q_B is 200–800 µs (92–94), and the half-time of PQ exchange of the Q_B site is approximately 10 ms (95). The OEC is thus kinetically limited by these downstream electron-transfer/exchange events and operates at a TOF much lower than its theoretical limit.

catalytic cycle involves four sequential P_{680} charge-separation events and four sequential OEC-oxidation events. The resulting OEC intermediates are known as S_i states ($i = 0$–4) (**Figure 2**). As first described by Kok et al. (6) on the basis of experiments by Joliot et al. (7), the OEC advances stepwise through the S_0, S_1, S_2, and S_3 states. When the S_3 state is advanced to the transient S_4 state, O_2 is spontaneously released and the S_0 state is reformed (6).

Significant progress, as described recently in several excellent reviews (14–17), has been made in understanding the structure and function of the OEC since the landmark discovery of period-four oscillations in O_2 production by Joliot and coworkers in 1969 (7). Herein, we discuss consensus models for states S_0–S_3 and their underlying inorganic and physical chemistry. However, an understanding of the mechanism of O–O bond formation has remained elusive to experimentalists. This great challenge of photosynthesis research motivates its discussion in this review and extensive efforts in laboratories throughout the world.
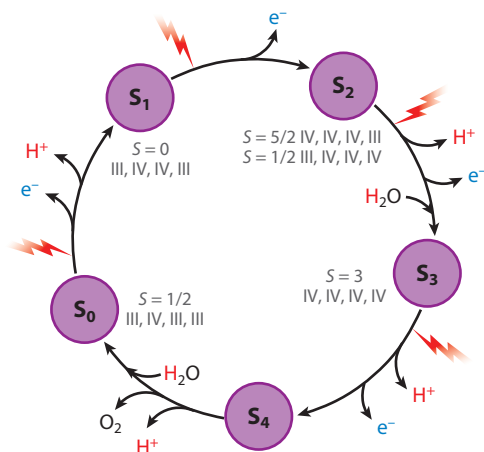
Figure 2

The redox intermediates in oxygen-evolving complex (OEC) catalysis are known as S_i states ($i = 0$–4), as first described by Kok et al. (6). Water enters the cycle in the $S_2 \rightarrow S_3$ (9, 10) and $S_4 \rightarrow S_0$ transitions (9). Protons are released in each S-state transition except $S_1 \rightarrow S_2$ (11, 12). The ground spin state (S) and Mn oxidation states (III, IV) are shown (13) for each state (for Mn numbering, see **Figure 1**).

STRUCTURE OF THE OXYGEN-EVOLVING COMPLEX

The OEC is an inorganic cluster of four Mn ions and one Ca ion connected by μ-oxo bridges (4, 5). As shown in **Figure 1**, the OEC can be described as a Mn_3CaO_4 hetero-cubane motif with a dangler Mn (notated Mn4) (18) connected to the cubane via an additional μ-oxo bridge (19). Amino acid residues (primarily carboxylate groups) make up the majority of the OEC ligands (20). In states S_0–S_2, Ca^{2+} and Mn4 each have two terminal water ligands (described below).

In 2011, a remarkable 1.9-Å resolution structure of PSII was produced by Shen and coworkers (**Figure 1**) (4). Unfortunately, all PSII X-ray crystal structures collected using conventional synchrotron radiation have suffered from radiation-induced Mn reduction (21). In 2014, the same research group produced a 1.95-Å resolution structure of PSII using a femtosecond X-ray free-electron laser method with the hope of avoiding radiation-induced reduction (22). However, model-dependent errors in the position of μ-oxo bridges likely arose from interpretation of electron-density maps when a light atom (O) was between several heavy atoms (Mn and Ca) (23). Nonetheless, X-ray diffraction structures have provided a crucial starting point toward building our modern understanding of the OEC structure. Extended X-ray absorption fine structure (EXAFS) data are much less prone to radiation-induced Mn reduction and provide reliable metal–metal and metal–ligand distance constraints (16, 24, 25). Electron paramagnetic resonance (EPR) and electron nuclear double resonance (ENDOR) data provide reliable spin-state assignments (26). Computational chemistry methods such as density functional theory (DFT) (e.g., 19) and quantum mechanics/molecular mechanics (QM/MM) (e.g., 27) have facilitated the combination of these datasets into the chemically reasonable structures that we discuss in the following sections.

ACCUMULATING HOLES AND REMOVING PROTONS

$S_0 \rightarrow S_1$

EPR and [55]Mn ENDOR data strongly suggest that the S_0 state, the most reduced OEC intermediate in the water-oxidation catalytic cycle, has a ground spin state of 1/2 (28–30) and does not contain a Mn^{2+} ion (31, 32). The spin states of the later S states (described in the following sections) thus require that the S_0 state contain $(Mn^{3+})_3Mn^{4+}$. DFT (9) and QM/MM (8) studies have assigned the Mn oxidation state pattern as III, IV, III, and III for Mn1, Mn2, Mn3, and Mn4, respectively (for atom numbering, see **Figures 1** and **3**). One μ-hydroxo bridge is present in S_0 and has been assigned to O5 (8, 9). However, continuum electrostatics methods have presented an alternative model with a Mn oxidation state pattern of III, III, IV, III and with O1 as a μ-hydroxo bridge (33).

In the OEC catalytic cycle, charge separation at P_{680} leads to oxidation of Y_Z, forming a neutral tyrosyl radical, $Y_Z^\bullet$, which in turn oxidizes S_0 to S_1. Starting from the dominant S_0 model, this conversion first involves the oxidation of Mn3 from Mn^{3+} to Mn^{4+}. This change causes the pK_a of O5 (a μ-hydroxo in S_0) to decrease dramatically. Although this pK_a change is challenging to measure, we can estimate a decrease of approximately 10 pH units for a μ-oxo bridging two Mn^{3+} centers versus one bridging Mn^{3+} and Mn^{4+} by analogy to the model complex $[Mn_2(\mu\text{-}O)_2(bpy)_4]^{2+/3+}$, where bpy represents 2,2′-bipyridine (34). Therefore, the proton on O5 is released following oxidation of S_0 (8, 35). Sequential oxidation and deprotonation results in an equivalent charge of the OEC in S_0 and in S_1 (35). The S_1 state contains the Mn oxidation state pattern III, IV, IV, III and is diamagnetic (36). As shown in **Figure 3**, all μ-oxo bridges are connected to at least one Mn^{4+} ion and are therefore deprotonated.
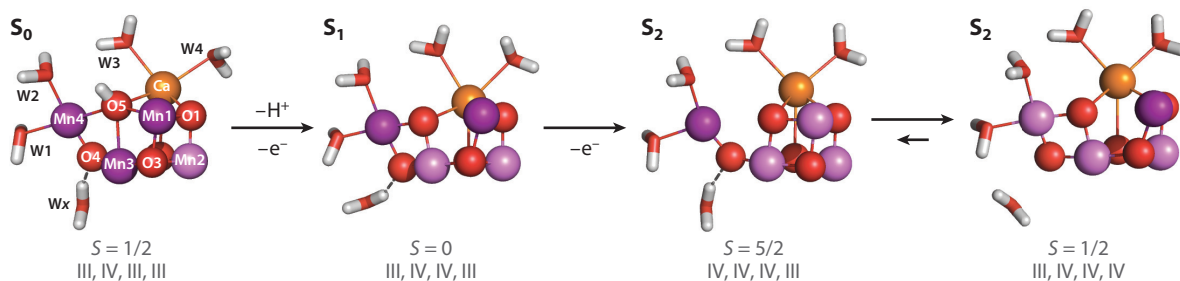
Figure 3

Quantum mechanics/molecular mechanics optimized structures of the S_0 (8), S_1 (8), S_2 ($S = 5/2$) (37), and S_2 ($S = 1/2$) (37) states from Batista, Brudvig and coworkers. Figure generated in PyMOL from coordinates in References 8 and 37. Comparable structures are presented in References 9 and 38–41. Mn^{3+} ions are shown in purple, Mn^{4+} in lavender, Ca^{2+} in orange, and O^{2-} in red.

$S_1 \rightarrow S_2$

The conversion of $Y_Z^\bullet S_1$ to $Y_Z S_2$ involves only an oxidation of the OEC (no proton release; see 11), and a positive charge is accumulated in the OEC during this transition (i.e., $S_1 \rightarrow S_2^+$) (35). The S_2 state can be generated from PSII preparations poised in the S_1 state either by a single-turnover flash at room temperature (42) or by continuous illumination at low temperature (130–220 K) (43, 44). The resulting S_2 state is paramagnetic and has been extensively studied using EPR spectroscopy (for reviews, see 45, 46). When the S_2 state is prepared in higher-plant PSII membranes by continuous illumination at <140 K, only a broad EPR signal at approximately $g = 4.1$ is observed (**Figure 4**) (44). When the same sample is warmed in complete darkness to >160 K, a dramatic multiline EPR signal at $g = 2$ is observed (**Figure 4**) (47). Both signals can also be generated by illumination of a sample poised in the S_1 state at about 200 K (43), but their relative intensities vary significantly depending on sample preparation (45).

The $g = 4.1$ and $g = 2$ EPR signals represent two spin isomers of the S_2 state (38, 48). The $g = 4.1$ signal corresponds to an isomer with a ground state of $S = 5/2$ (49, 50) and with a Mn oxidation state pattern of IV, IV, IV, III (38). In this closed cubane form of the S_2 state, the dangler Mn4 is a five-coordinate Mn^{3+} center and is weakly electronically coupled to the other three Mn^{4+} ions in the cubane motif. Spin frustration in the trigonal cuboidal motif promotes a high spin state. The $g = 2$ signal corresponds to an isomer with a ground state of $S = 1/2$ (42) and with a Mn oxidation state pattern of III, IV, IV, IV (38). In this open cubane form, Mn1 is a five-coordinate Mn^{3+} center. Di-μ-oxo bridges connect all Mn ions, resulting in short Mn–Mn distances. This linear arrangement of pairs promotes antiferromagnetic coupling and a low spin state.

We have hypothesized that the S_2 state $S = 5/2$ spin isomer is the direct product of S_1 oxidation, as shown in **Figure 3** (51). However, the $S = 1/2$ spin isomer has a slightly lower reduction potential, as observed experimentally in spinach PSII membranes using sucrose as a cryoprotectant (0.7 ± 0.1 kcal/mol) (51) and predicted computationally (0.4–1.6 kcal/mol) (38, 39, 41, 52). Therefore, at room temperature, the equilibrium constant of the S_2 state spin isomers (defined here as [$S = 1/2$]/[$S = 5/2$]) is approximately 3 in spinach PSII membranes under the conditions measured. The relative abundance of each spin isomer is sensitive to PSII preparation (e.g., cyanobacterial PSII core complexes versus higher-plant PSII membranes), choice of cryoprotectant, Cl^- concentration, and presence of small molecules such as acetate, ammonia, and methanol (for a review, see 45).

S: ground spin state
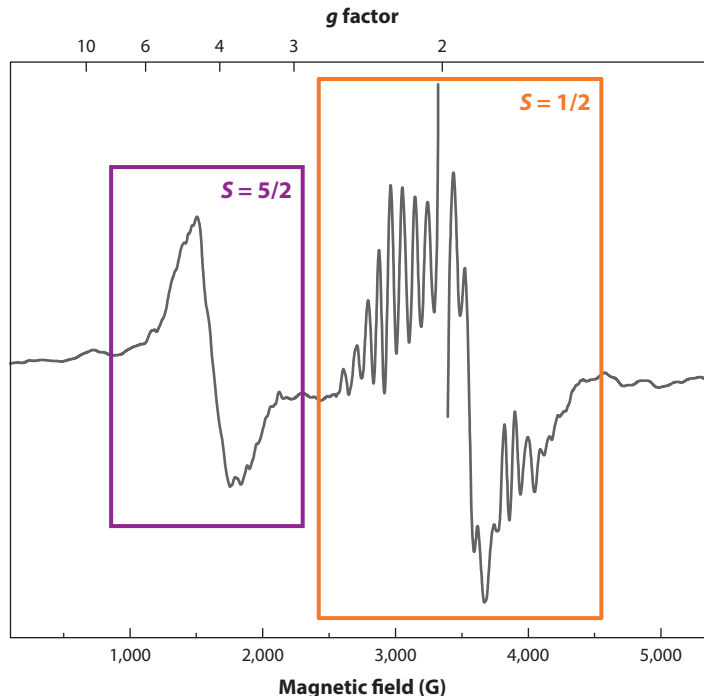
Figure 4

X-band electron paramagnetic resonance spectrum of the S_2 state in higher-plant PSII membranes in a sucrose-containing buffer at 7 K. The broad signal centered at $g = 4.1$ (*purple box*) arises from the S_2 population with a ground spin state of $S = 5/2$. The multiline signal centered at $g = 2$ (*orange box*) arises from the S_2 population with a ground spin state of $S = 1/2$.

$S_2 \rightarrow S_3$

The conversion of $Y_Z{}^\bullet S_2$ to $Y_Z S_3$ involves deprotonation, Mn oxidation, and water coordination (10, 35). The resulting S_3 state's Mn centers are all six-coordinate Mn^{4+} centers (10), as shown in **Figure 5**. Although a consensus has emerged for the structure of the S_3 state (discussed below), the mechanism of its formation from the S_2 state is still debated. Three proposed mechanisms are shown in **Figure 5**. Siegbahn (9) first showed using DFT calculations that an OEC containing all Mn^{4+} centers required an additional ligand compared to the S_2 state, and this was confirmed by experiment (10). Siegbahn's mechanism (**Figure 5a**) starts from the open cubane $S = 1/2$ spin isomer of the S_2 state and involves a new water molecule added to Mn1 when it is oxidized from Mn^{3+} to Mn^{4+}. This water is deprotonated to form a terminal hydroxo ligand.

Several computational groups, including Yamaguchi and coworkers (40), Guidoni and coworkers (41), and Kaila and coworkers (39), have suggested that a water molecule is transferred from Ca^{2+} to Mn4 during this transition. This mechanism (**Figure 5b**) starts from the closed cubane $S = 5/2$ spin isomer of the S_2 state. W3 moves to Mn4 when it is oxidized from Mn^{3+} to Mn^{4+}. A water molecule from the hydrogen-bonded network surrounding the OEC binds to Ca^{2+} at the site previously occupied by W3.

A third mechanism was inspired by studies of ammonia binding to the S_2 state (for a review, see 53) and involves water molecules moving around the Mn4 center. As shown in **Figure 5c**, a second-shell water molecule denoted by Wx is a hydrogen-bond donor to O4 in the closed cubane $S = 5/2$ spin isomer of the S_2 state. We proposed that upon formation of the S_3 state, Wx becomes
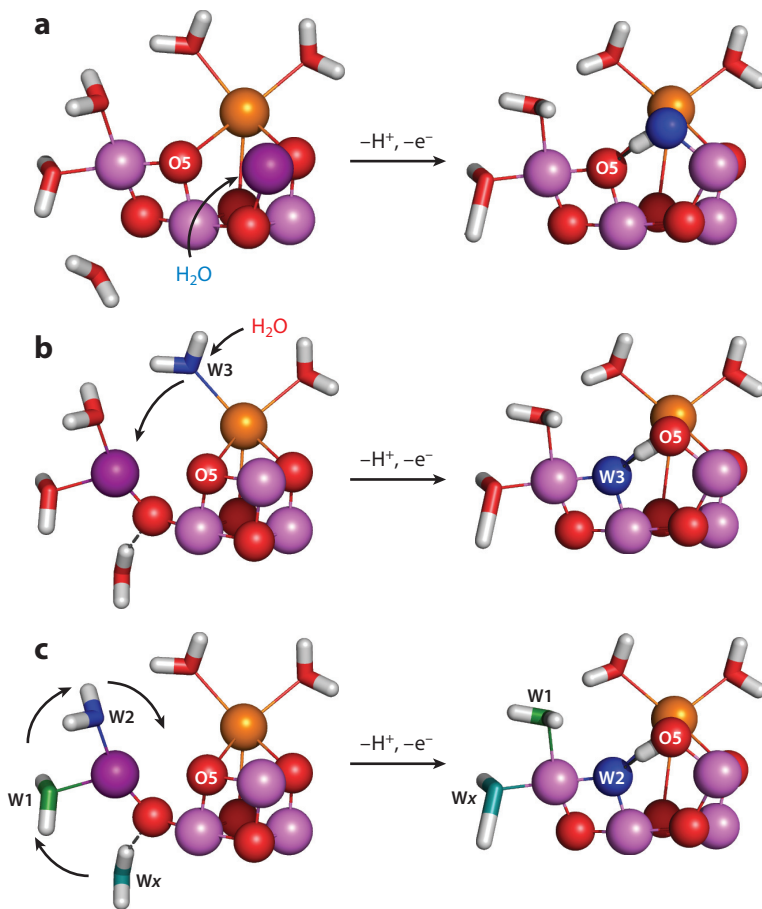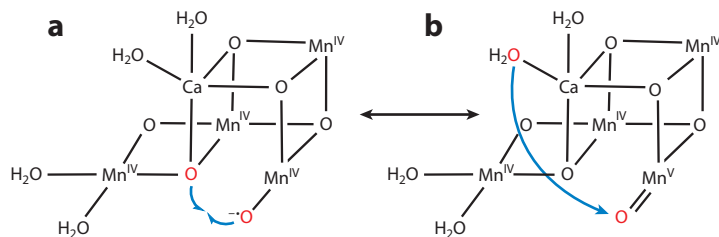
Figure 5

Models for conversion of the S_2 state to the S_3 state. (*a*) External water addition to Mn1 as proposed by Siegbahn (9). (*b*) Transfer of water from Ca^{2+} to Mn4 as proposed by Yamaguchi and coworkers (40), Guidoni and coworkers (41), and Kaila and coworkers (39). (*c*) Carousel or pivot movement of water around Mn4 as proposed by Brudvig, Batista and coworkers (37), Pantazis, Cox and coworkers (54), and Guidoni and coworkers (55).

a direct ligand to the dangler Mn, causing W1 and W2 to be displaced in a carousel around Mn4 (37). Pantazis, Cox and coworkers (54) later proposed an equivalent pivot mechanism (see also 55). Note that in both the mechanisms shown in **Figure 5*b,c***, O5 is converted from a μ-oxo bridge to a terminal hydroxo. W3 (**Figure 5*b***) or W2 (**Figure 5*c***) is converted from a terminal water ligand to a μ-oxo bridge.

As does the S_2 state, the S_3 state decays to the S_1 state in darkness via charge recombination with electrons from the acceptor side of PSII (56, 57). The S_3 state is, however, significantly more resistant to small molecule reductants such as hydrazine or hydroxylamine than the S_2 state (58). This behavior is likely the result of each Mn center in the S_3 state being in a coordinatively saturated octahedral Mn^{4+} oxidation state (10), whereas in the S_2 state one Mn center is a five-coordinate Mn^{3+} that is accessible to ligand binding and inner-sphere reaction (38).

Figure 6

Proposed mechanisms for O–O bond formation upon formation of the S_4 state. (*a*) A Mn^{4+}–$O^\bullet$ species in the S_4 state could give rise to an oxo–oxyl radical attack mechanism. (*b*) A Mn^{5+}=O species in the S_4 state could give rise to a water-nucleophile attack mechanism.

O–O BOND FORMATION

$S_3 \rightarrow [S_4] \rightarrow S_0$

Experimental data for the $S_3 \rightarrow S_0$ transition are scarce. Formally, this process must involve the release of two protons, O_2 formation and release, and a water-binding event (35). Time-resolved X-ray fluorescence experiments have shown that when a single-turnover flash is applied to PSII membranes poised in the S_3 state, a $Y_Z^\bullet S_3'$ intermediate persists for approximately 250 μs before Mn reduction is observed, which is rapidly followed by O_2 release and S_0 state formation (59). This lag phase is pH dependent and has an H/D isotope effect, which strongly suggests that it represents a proton release (60). In these time-resolved Mn K-edge X-ray spectroscopy experiments, no Mn oxidation event is observed subsequent to formation of the $Y_Z^\bullet S_3'$ intermediate (59), which suggests either that the final hole transfer is not Mn centered or that a Mn^{5+} intermediate decays faster than it is formed. Siegbahn (9, 19) has championed an S_4 state containing a Mn^{4+}-oxyl center (**Figure 6a**). An alternative S_4 state, proposed by Pecoraro and coworkers (61) and Brudvig and coworkers (62, 63), contains a Mn^{5+}-oxo center (**Figure 6b**). Both of these S_4 states are isoelectronic. A Mn^{4+}-oxyl species adjacent to a μ-oxo bridge (with correct spin states; see 64) could give rise to an oxo–oxyl radical coupling mechanism for O–O bond formation. However, a Mn^{5+}=O center is predicted to be highly electrophilic and could give rise to a water-nucleophile attack mechanism for O–O bond formation. The former mechanism has been supported by extensive computational studies (e.g., 9). The latter mechanism is analogous to most well-described inorganic water-oxidation catalysts (for a review, see 65). As shown in **Figure 6**, we favor the assignment of the nucleophile to a terminal water on Ca^{2+} (W3). Although a free hydroxide is a better nucleophile, it has high electrostatic binding energy to the metal center, which renders a hydroxide ligand to a high-valent metal ion less nucleophilic. However, if the pK_a of a nucleophilic water is tuned to a value close to the ambient pH, it can simultaneously attack the electrophile and be deprotonated. Because water bound to Ca^{2+} is more acidic than bulk water (66), it is an excellent candidate for this mechanism. To date, however, neither the oxo–oxyl radical mechanism nor the water-nucleophile attack mechanism for the OEC has been supported or rejected by experimental evidence.

It is likely an oversimplification to notate the S_4 state formally as either Mn^{4+}–$O^\bullet$ or Mn^{5+}=O. Instead, the hole is almost certainly delocalized between Mn and O. In the S_4 state predicted by Li & Siegbahn (67), the spin population on O was calculated to be approximately 0.7. In a Mn^{5+}=O model complex recently prepared by Borovik and coworkers (68, 69), the spin population on O was measured by EPR spectroscopy to be approximately 0.45. Subtle changes both within the

HOW EFFICIENT IS PSII?

Although the photochemical quantum yield of PSII approaches 100% (96), its net solar-to-chemical energy conversion efficiency is significantly lower (71). The production of one molecule of O_2 requires four charge-separation events. Assuming that four 680-nm photons are sequentially absorbed by P_{680}, the solar energy input is 4×1.83 eV, or 7.32 eV. The reduction potential of Q_B^-/Q_B, the terminal electron acceptor of PSII, is $+0.09$ V (97). The reduction potential of H_2O/O_2, the electron donor of PSII, is $+0.88$ V at pH 6.0 (98). Consequently, the chemical energy change in each PSII turnover is $4 \times (+0.09 - 0.88)$ eV or -3.16 eV. Each PSII turnover also pumps eight protons across the thylakoid membrane (four protons are released to the lumen from the oxidation of water, and four protons are consumed from the stroma from the reduction of PQ). Assuming a proton-to-ATP ratio of 4.67 for the chloroplast ATPase (99), 1.71 ATP are formed for each molecule of O_2, corresponding to a change of -0.56 eV in chemical energy (100).

Therefore, of the 7.32 eV of solar energy that enters PSII, approximately 3.72 eV, or 50.8%, is converted to chemical energy (3.16 eV from reaction center chemistry plus 0.56 eV from ATP production). This calculation implies that approximately half of the input solar energy is used to overcome activation barriers and/or is released to the surroundings as heat.

OEC and in its local environment will likely propagate into large differences in the spin density distribution between Mn and O in the S_4 state and will, therefore, influence the electronics of O–O bond formation.

Proton-Coupled Electron Transfer in the Oxygen-Evolving Complex

As described above, the $Y_Z S_0 \rightarrow Y_Z^\bullet S_3$ transitions involve alternating oxidation and deprotonation steps, and all of the redox transitions occur within a narrow range of reduction potentials. This redox leveling is responsible for maintaining the low overpotential requirement of the OEC (70–72). However, it is possible that the final oxidation step, in which the S_4 state is formed, is a concerted proton-coupled electron transfer (PCET). Such a mechanism would involve a proton transfer ($Y_Z^\bullet S_3 \rightarrow Y_Z^\bullet S_3'$) followed by a low-barrier PCET ($Y_Z^\bullet S_3' \rightarrow Y_Z S_4$). Such PCET strategies for lowering activation barriers are widely used in other redox-active enzymes (73). See the sidebar titled How Efficient Is PSII? for a discussion of the overall efficiency of PSII.

RATIONALIZING SUBSTRATE WATER EXCHANGE KINETICS

The Wydrzynski laboratory first developed a method to measure the rates at which $H_2^{18}O$ exchanges with substrate waters in each S state (for reviews, see 14, 74). The resulting data (**Table 1**) are crucial for understanding the mechanism of PSII water oxidation, but have been difficult to rationalize with the chemical structures of the S states.

In the S_0 and S_1 states, only one substrate water exchange rate is resolved. This result implies either that the second substrate water is not bound to the OEC in these intermediates or that it exchanges at a rate faster than the experiment can detect. The exchange rate of the slow water decreases 500-fold in the $S_0 \rightarrow S_1$ transition (**Table 1**).

Two substrate water exchange rates are observed in the S_2 (77) and S_3 (78) states. The slow water exchanges at the same rate in both states, but, surprisingly, this rate is 100-fold faster than the rate of exchange in the S_1 state. The fast water exchanges at a rate of approximately 120 s^{-1} in the S_2 state and slows to 40 s^{-1} in the S_3 state (**Table 1**).

PCET:
proton-coupled
electron transfer

Table 1 **Rates of fast (k_f) and slow (k_s) substrate water exchange at 10°C in spinach thylakoid membranes (75, 76)**

	k_s (s^{-1})	k_f (s^{-1})
S_0	10	>120
S_1	0.02	>120
S_2	2	120
S_3	2	40

Exchange of a μ-Oxo Bridge Adjacent to a Terminal Water in the Oxygen-Evolving Complex

Researchers (14, 79, 80) including ourselves (81) have argued that the slow-exchanging water in the S_0 and S_1 states represents the exchange of the μ-oxo bridge O5. Both the exchange of a μ-hydroxo bridge between two Mn^{3+} centers (analogous to S_0) and the exchange of a μ-oxo bridge between one Mn^{3+} and one Mn^{4+} center (analogous to S_1) have been observed in model complexes (82, 83). The O5 position is of particular interest in that it is adjacent to a terminal water ligand bound to Mn4. We present a proposed mechanism of O5 exchange in the S_1 state in **Figure 7** on the basis of results from μ-oxo exchange in inorganic complexes (83). In this model, the terminal water ligand W2 on the dangler Mn4 is exchanged with two rates. The first rate is fast and represents direct water exchange (**Figure 7**, reaction ❶). The second rate is slower and represents the equilibrium between the ^{18}O label in the O5 and W2 positions (**Figure 7**, reactions ❶–❹).
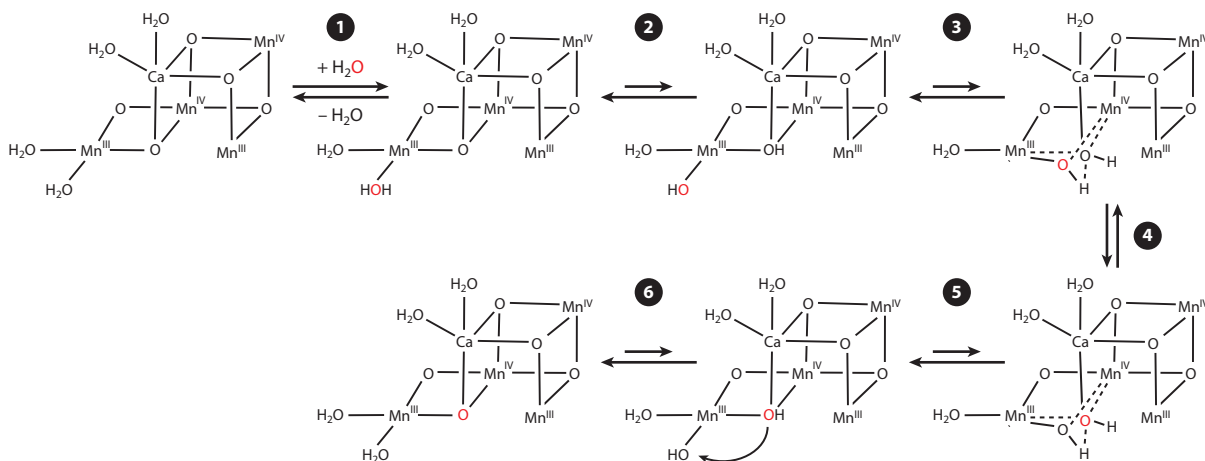
Figure 7

A proposed chemical mechanism for the exchange of O5 with $H_2^{18}O$ (*red*). Reaction ❶: Exchange of a terminal water ligand on a Mn^{III} center is facile, especially if the ligand is on the Jahn–Teller axis (84). Reaction ❷: A μ-oxo bridge must be protonated before dissociation (83). By analogy to model complexes, the pK_a of O5 bridging one Mn^{III} and one Mn^{IV} is several pH units below physiological pH (82), and water bound as a terminal ligand to Mn^{III} is acidic (85), which facilitates proton transfer from a terminal water ligand to O5. Reaction ❸: Once protonated, (OH)5 partially dissociates from one or both Mn centers and forms a hydrogen bond with the labeled terminal water. Reaction ❹: This hydrogen-bonded network facilitates exchange of the isotopically labeled oxygen atom between the two positions (83). This equilibrium effectively scrambles the label between the W2 and O5 positions. Reaction ❺: (OH)5 reforms the formal μ-hydroxo bridge between the two Mn centers, and the hydrogen bond with the terminal water ligand is broken. Reaction ❻: The low pK_a of (OH)5 results in its facile deprotonation to complete the ^{18}O exchange.

Table 2 Potential identities of the oxygen-evolving complex substrate waters on the basis of the mechanism of $S_2 \rightarrow S_3$ water delivery and O–O bond formation; for O numbering, see Figure 1

S₂ → S₃ mechanism	O–O bond formation mechanism	
	Oxo–oxyl radical coupling (9, 19)	**Water-nucleophile attack (61–63)**
External water addition (**Figure 5a**) (9)	O5 + outside water	W3 + outside water
Ca²⁺-mediated water addition (**Figure 5b**) (39–41)	O5 + W3	W3 + O5
Carousel or pivot around Mn4 (**Figure 5c**) (37, 54, 55)	O5 + W2	W3 + O5

The exchange of a μ-oxo bridge is possible only when it can be protonated and can, therefore, dissociate from at least one of the Mn centers (83). In the model complex $[Mn_2^{III,III}(\mu\text{-}O)_2(bpy)_4]^{2+}$, the pK_a of the μ-oxo is approximately 12 (34) and is, therefore, predominantly protonated at neutral pH. For $[Mn_2^{III,IV}(\mu\text{-}O)_2(bpy)_4]^{3+}$, the μ-oxo pK_a decreases to approximately 2 (82), and for $[Mn_2^{IV,IV}(\mu\text{-}O)_2(bpy)_4]^{4+}$, it has been estimated to be approximately −6 (34). This trend suggests that O5 exchanges readily in the S_0 state (adjacent to two Mn^{3+} ions) and exchanges much more slowly in the S_1 state (adjacent to one Mn^{3+} ion and one Mn^{4+} ion) (14, 81). These comparisons are qualitatively consistent with the exchange rates for slow water shown in **Table 1** for S_0 and S_1, respectively. In the S_2 state, O5 is adjacent to two Mn^{4+} ions. On the basis of inorganic chemistry precedent, one would, therefore, expect the rate of O5 exchange in the S_2 state (μ-oxo adjacent to two Mn^{4+} ions) to be several orders of magnitude slower than in the S_1 state. However, the exchange rate of the slow water instead increases 100-fold in the $S_1 \rightarrow S_2$ transition. We have interpreted this unusual observation as suggesting that the observed exchange rate for slow water reflects the slow phase of a terminal water (W2) being labeled via exchange with O5 in the S_0 and S_1 states (**Figure 7**) and reflects the direct exchange of a terminal water in the S_2 and S_3 states (81).

Which Waters Are Substrate Waters?

In two of the mechanisms for water delivery to the S_3 state from the S_2 state (**Figure 5b,c**), the oxygen atom O5 is converted from a μ-oxo bridge to a terminal hydroxo ligand on a Mn^{4+} ion. Such a transition would substantially increase its exchange rate. In the mechanism for water delivery shown in **Figure 5a**, one of the substrate waters is not bound in the S_2 state, which is likely in contradiction to experimental data.

Table 2 summarizes the possible identities of the two substrate waters in the OEC on the basis of both the $S_2 \rightarrow S_3$ water delivery mechanism (**Figure 5**) and the O–O bond formation mechanism (**Figure 6**). At this time, it is not possible to confirm any of the entries in **Table 2**. Instead, we present this discussion of O–O bond formation and $S_2 \rightarrow S_3$ water delivery mechanisms as a foundation for the development of new experiments to test these hypotheses.

SUMMARY POINTS

- The OEC in PSII is the source of nearly all O_2 on Earth, yet a complete chemical mechanism of water oxidation has not been established.

- Multiple experimental and computational groups have arrived at consensus structures of the S_0, S_1, S_2, and S_3 intermediates of the OEC.
- In the $S_2 \rightarrow S_3$ transition, a new water molecule is added to the OEC, but multiple mechanisms are still being discussed.
- The S_4 state likely contains either a Mn^{4+}–$O^\bullet$ species or a $Mn^{5+} = O$ species. The former could give rise to an oxo–oxyl radical mechanism for O–O bond formation, whereas the latter could lead to a water-nucleophile attack mechanism.
- Inorganic chemistry precedent strongly suggests that a μ-oxo bridge cannot exchange fast enough to account for the millisecond kinetics of substrate exchange in the S_2 and S_3 states, which provides a constraint on the binding modes of substrate waters proposed in mechanistic models.

FUTURE ISSUES

- Much of our understanding of O–O bond formation comes from computational studies. What experiments could be designed to confirm or reject hypotheses generated from theory? Are structural studies (e.g. femtosecond X-ray crystallography) or spectroscopic studies (e.g. EXAFS, EPR) more likely to provide these insights?
- What are the exact assignments of the substrate water exchange kinetics? How does this inform the mechanism of O–O bond formation?
- How can a detailed knowledge of OEC chemistry inform the design of synthetic catalysts for efficient water oxidation?

DISCLOSURE STATEMENT

The authors are not aware of any affiliations, memberships, funding, or financial holdings that might be perceived as affecting the objectivity of this review.

ACKNOWLEDGMENTS

LITERATURE CITED

4. In this PSII X-ray crystal structure study at 1.9-Å resolution, all atoms of the OEC were resolved for the first time.

1. Blankenship RE. 2014. *Molecular Mechanisms of Photosynthesis*. Chichester, UK: Wiley-Blackwell
2. Falkowski PG, Raven JA. 2007. *Aquatic Photosynthesis*. Princeton, NJ: Princeton Univ. Press
3. Vinyard DJ, Ananyev GM, Dismukes GC. 2013. Photosystem II: the reaction center of oxygenic photosynthesis. *Annu. Rev. Biochem.* 82:577–606
4. **Umena Y, Kawakami K, Shen J-R, Kamiya N. 2011. Crystal structure of oxygen-evolving photosystem II at a resolution of 1.9 Å. *Nature* 473:55–60**

5. Ferreira K, Iverson T, Maghlaoui K, Barber J, Iwata S. 2004. Architecture of the photosynthetic oxygen-evolving center. *Science* 303:1831–38

6. Kok B, Forbush B, McGloin M. 1970. Cooperation of charges in photosynthetic O_2 evolution. I. A linear four step mechanism. *Photochem. Photobiol.* 11:457–75

7. Joliot P, Barbieri G, Chabaud R. 1969. Un nouveau modèle des centres photochimiques du système II. *Photochem. Photobiol.* 10:309–29

8. Pal R, Negre CFA, Vogt L, Pokhrel R, Ertem MZ, et al. 2013. S_0-state model of the oxygen-evolving complex of photosystem II. *Biochemistry* 52:7703–6

9. Siegbahn PEM. 2013. Water oxidation mechanism in photosystem II, including oxidations, proton release pathways, O–O bond formation and O_2 release. *Biochim. Biophys. Acta* 1827:1003–19

10. Cox N, Retegan M, Neese F, Pantazis DA, Boussac A, Lubitz W. 2014. Electronic structure of the oxygen-evolving complex in photosystem II prior to O–O bond formation. *Science* 345:804–8

11. Schlodder E, Witt HT. 1999. Stoichiometry of proton release from the catalytic center in photosynthetic water oxidation: reexamination by a glass electrode study at pH 5.5–7.2. *J. Biol. Chem.* 274:30387–92

12. Lavergne J, Junge W. 1993. Proton release during the redox cycle of the water oxidase. *Photosynth. Res.* 38:279–96

13. Krewald V, Retegan M, Cox N, Messinger J, Lubitz W, et al. 2015. Metal oxidation states in biological water splitting. *Chem. Sci.* 6:1676–95

14. Cox N, Messinger J. 2013. Reflections on substrate water and dioxygen formation. *Biochim. Biophys. Acta* 1827:1020–30

15. Shen J-R. 2015. The structure of photosystem II and the mechanism of water oxidation in photosynthesis. *Annu. Rev. Plant Biol.* 66:23–48

16. Yano J, Yachandra V. 2014. Mn_4Ca cluster in photosynthesis: where and how water is oxidized to dioxygen. *Chem. Rev.* 114:4175–205

17. Pérez-Navarro M, Neese F, Lubitz W, Pantazis DA, Cox N. 2016. Recent developments in biological water oxidation. *Curr. Opin. Chem. Biol.* 31:113–19

18. Peloquin JM, Campbell KA, Randall DW, Evanchik MA, Pecoraro VL, et al. 2000. [55]Mn ENDOR of the S_2-state multiline EPR signal of photosystem II: implications on the structure of the tetranuclear Mn cluster. *J. Am. Chem. Soc.* 122:10926–42

19. Siegbahn PEM. 2008. A structure-consistent mechanism for dioxygen formation in photosystem II. *Chem. Eur. J.* 14:8290–302

20. Debus RJ. 2008. Protein ligation of the photosynthetic oxygen-evolving center. *Coord. Chem. Rev.* 252:244–58

21. Yano J, Kern J, Irrgang KD, Latimer MJ, Bergmann U, et al. 2005. X-ray damage to the Mn_4Ca complex in single crystals of photosystem II: a case study for metalloprotein crystallography. *PNAS* 102:12047–52

22. Suga M, Akita F, Hirata K, Ueno G, Murakami H, et al. 2014. Native structure of photosystem II at 1.95 Å resolution viewed by femtosecond X-ray pulses. *Nature* 517:99–103

23. Askerka M, Vinyard DJ, Wang J, Brudvig GW, Batista VS. 2015. Analysis of the radiation-damage-free X-ray structure of photosystem II in light of EXAFS and QM/MM data. *Biochemistry* 54:1713–16

24. Grundmeier A, Dau H. 2012. Structural models of the manganese complex of photosystem II and mechanistic implications. *Biochim. Biophys. Acta* 1817:88–105

25. Haumann M, Müller C, Liebisch P, Iuzzolino L, Dittmer J, et al. 2005. Structural and oxidation state changes of the photosystem II manganese complex in four transitions of the water oxidation cycle ($S_0 \rightarrow S_1$, $S_1 \rightarrow S_2$, $S_2 \rightarrow S_3$, $S_{3,4} \rightarrow S_0$) characterized by X-ray absorption spectroscopy at 20 K and room temperature. *Biochemistry* 44:1894–908

26. Krewald V, Retegan M, Neese F, Lubitz W, Pantazis DA, Cox N. 2016. Spin state as a marker for the structural evolution of nature's water-splitting catalyst. *Inorg. Chem.* 55:488–501

27. Luber S, Rivalta I, Umena Y, Kawakami K, Shen J-R, et al. 2011. S_1-state model of the O_2-evolving complex of photosystem II. *Biochemistry* 50:6308–11

28. Åhrling KA, Peterson S, Styring S. 1997. An oscillating manganese electron paramagnetic resonance signal from the S_0 state of the oxygen evolving complex in photosystem II. *Biochemistry* 36:13148–52

29. Messinger J, Nugent JHA, Evans MCW. 1997. Detection of an EPR multiline signal for the S_0 state in photosystem II. *Biochemistry* 36:11055–60

5. This landmark PSII X-ray crystal structure study at 3.5-Å resolution laid the groundwork for a detailed understanding of OEC structure.

9. This is an excellent review of the author's extensive DFT studies of OEC structure and the O–O bond formation mechanism.

30. Messinger J, Robblee JH, Yu WO, Sauer K, Yachandra VK, Klein MP. 1997. The S_0 state of the oxygen-evolving complex in photosystem II is paramagnetic: detection of an EPR multiline signal. *J. Am. Chem. Soc.* 119:11349–50

31. Kulik LV, Epel B, Lubitz W, Messinger J. 2005. ^{55}Mn pulse ENDOR at 34 GHz of the S_0 and S_2 states of the oxygen-evolving complex in photosystem II. *J. Am. Chem. Soc.* 127:2392–93

32. Kulik LV, Epel B, Lubitz W, Messinger J. 2007. Electronic structure of the Mn_4O_xCa cluster in the S_0 and S_2 states of the oxygen-evolving complex of photosystem II based on pulse ^{55}Mn-ENDOR and EPR spectroscopy. *J. Am. Chem. Soc.* 129:13421–35

33. Amin M, Vogt L, Szejgis W, Vassiliev S, Brudvig GW, et al. 2015. Proton-coupled electron transfer during the S-state transitions of the oxygen-evolving complex of photosystem II. *J. Phys. Chem. B* 119:7366–77

34. **Amin M, Vogt L, Vassiliev S, Rivalta I, Sultan MM, et al. 2013. Electrostatic effects on proton coupled electron transfer in oxomanganese complexes inspired by the oxygen-evolving complex of photosystem II. *J. Phys. Chem. B* 117:6217–26**

35. Dau H, Haumann M. 2007. Eight steps preceding O–O bond formation in oxygenic photosynthesis—a basic reaction cycle of the photosystem II manganese complex. *Biochim. Biophys. Acta* 1767:472–83

36. Koulougliotis D, Hirsh DJ, Brudvig GW. 1992. The oxygen-evolving center of photosystem II is diamagnetic in the S_1 resting state. *J. Am. Chem. Soc.* 114:8322–23

37. **Askerka M, Vinyard DJ, Brudvig GW, Batista VS. 2015. NH_3 binding to the S_2 state of the O_2-evolving complex of photosystem II: analogue to H_2O binding during the $S_2 \rightarrow S_3$ transition. *Biochemistry* 54:5783–86**

38. **Pantazis DA, Ames W, Cox N, Lubitz W, Neese F. 2012. Two interconvertible structures that explain the spectroscopic properties of the oxygen-evolving complex of photosystem II in the S_2 state. *Angew. Chem. Int. Ed.* 51:9935–40**

39. Ugur I, Rutherford AW, Kaila VRI. 2016. Redox-coupled substrate water reorganization in the active site of photosystem II—the role of calcium in substrate water delivery. *Biochim. Biophys. Acta* 1857:740–48

40. Shoji M, Isobe H, Yamaguchi K. 2015. QM/MM study of the S_2 to S_3 transition reaction in the oxygen-evolving complex of photosystem II. *Chem. Phys. Lett.* 636:172–79

41. Bovi D, Narzi D, Guidoni L. 2013. The S_2 state of the oxygen-evolving complex of photosystem II explored by QM/MM dynamics: Spin surfaces and metastable states suggest a reaction path towards the S_3 state. *Angew. Chem. Int. Ed.* 52:11744–49

42. Dismukes GC, Siderer Y. 1981. Intermediates of a polynuclear manganese center involved in photosynthetic oxidation of water. *PNAS* 78:274–78

43. de Paula JC, Innes JB, Brudvig GW. 1985. Electron transfer in photosystem II at cryogenic temperatures. *Biochemistry* 24:8114–20

44. Casey JL, Sauer K. 1984. EPR detection of a cryogenically photogenerated intermediate in photosynthetic oxygen evolution. *Biochim. Biophys. Acta* 767:21–28

45. Pokhrel R, Brudvig GW. 2014. Oxygen-evolving complex of photosystem II: correlating structure with spectroscopy. *Phys. Chem. Chem. Phys.* 16:11812–21

46. Haddy A. 2007. EPR spectroscopy of the manganese cluster of photosystem II. *Photosynth. Res.* 92:357–68

47. de Paula JC, Beck WF, Miller A-F, Wilson RB, Brudvig GW. 1987. Studies of the manganese site of photosystem II by electron spin resonance spectroscopy. *J. Chem. Soc. Faraday Trans.* 83:3635–51

48. Zimmermann JL, Rutherford AW. 1986. Electron paramagnetic resonance properties of the S_2 state of the oxygen-evolving complex of photosystem II. *Biochemistry* 25:4609–15

49. Haddy A, Lakshmi KV, Brudvig GW, Frank HA. 2004. Q-band EPR of the S_2 state of photosystem II confirms an $S = 5/2$ origin of the X-band $g = 4.1$ signal. *Biophys. J.* 87:2885–96

50. Astashkin AV, Kodera Y, Kawamori A. 1994. Pulsed EPR study of manganese $g = 4.1$ signal in plant photosystem II. *J. Magn. Reson. B* 105:113–19

51. Vinyard DJ, Khan S, Askerka M, Batista VS, Brudvig GW. 2017. Energetics of the S_2 state spin isomers of the oxygen-evolving complex of photosystem II. *J. Phys. Chem. B* 121:1020–25

52. Isobe H, Shoji M, Shen J-R, Yamaguchi K. 2015. Strong coupling between the hydrogen bonding environment and redox chemistry during the S_2 to S_3 transition in the oxygen-evolving complex of photosystem II. *J. Phys. Chem. B* 119:13922–33

34. Continuum electrostatics methods allowed accurate predictions of pK_a values for both terminal water and μ-oxo ligands in Mn model complexes.

37. Studies of ammonia binding to the S_2 state inspired a new carousel mechanism of water binding to the S_3 state.

38. DFT methods were used to show how decades of EPR data could be reconciled by two spin isomers of the S_2 state having different Mn^{3+} and O5 positions.

53. Askerka M, Brudvig GW, Batista VS. 2017. The O_2-evolving complex of photosystem II: recent insights from quantum mechanics/molecular mechanics (QM/MM), extended X-ray absorption fine structure (EXAFS), and femtosecond X-ray crystallography data. *Acc. Chem. Res.* 50:41–48

54. Retegan M, Krewald V, Mamedov F, Neese F, Lubitz W, et al. 2016. A five-coordinate Mn(IV) intermediate in biological water oxidation: spectroscopic signature and a pivot mechanism for water binding. *Chem. Sci.* 7:72–84

55. Capone M, Narzi D, Bovi D, Guidoni L. 2016. Mechanism of water delivery to the active site of photosystem II along the S_2 to S_3 transition. *J. Phys. Chem. Lett.* 7:592–96

56. Lavergne J, Étienne A-L. 1980. Prompt and delayed fluorescence of chloroplasts upon mixing with dichlorophenyldimethylurea. *Biochim. Biophys. Acta* 593:136–48

57. Rutherford AW, Inoue Y. 1984. Oscillation of delayed luminescence from PSII: recombination of $S_2Q_B^-$ and $S_3Q_B^-$. *FEBS Lett.* 165:163–70

58. Messinger J, Wacker U, Renger G. 1991. Unusual low reactivity of the water oxidase in redox state S_3 toward exogenous reductants. Analysis of the NH_2OH- and NH_2NH_2-induced modifications of flash-induced oxygen evolution in isolated spinach thylakoids. *Biochemistry* 30:7852–62

59. Haumann M, Liebisch P, Müller C, Barra M, Grabolle M, Dau M. 2005. Photosynthetic O_2 formation tracked by time-resolved X-ray experiments. *Science* 310:1019–21

60. Gerencsér L, Dau H. 2010. Water oxidation by photosystem II: $H_2O–D_2O$ exchange and the influence of pH support formation of an intermediate by removal of a proton before dioxygen creation. *Biochemistry* 49:10098–106

61. Pecoraro VL, Baldwin MJ, Caudle MT, Hsieh W-Y, Law NA. 1998. A proposal for water oxidation in photosystem II. *Pure Appl. Chem.* 70:925–29

62. Brudvig GW. 2008. Water oxidation chemistry of photosystem II. *Philos. Trans. R. Soc. B* 363:1211–19

63. Szalai VA, Stone DA, Brudvig GW. 1998. A structural and mechanistic model of the O_2-evolving complex of photosystem II. In *Photosynthesis: Mechanisms and Effects*, ed. G Garab, pp. 1403–6. Dordrecht, Neth.: Kluwer Academic

64. Siegbahn PEM. 2011. Recent theoretical studies of water oxidation in photosystem II. *J. Photochem. Photobiol. B* 104:94–99

65. Romain S, Vigara L, Llobet A. 2009. Oxygen–oxygen bond formation pathways promoted by ruthenium complexes. *Acc. Chem. Res.* 42:1944–53

66. Dean JA. 1985. *Lange's Handbook of Chemistry*. New York: McGraw-Hill

67. Li X, Siegbahn PEM. 2015. Water oxidation for simplified models of the oxygen-evolving complex in photosystem II. *Chem. Eur. J.* 21:18821–27

68. Gupta R, Taguchi T, Lassalle-Kaiser B, Bominaar EL, Yano J, et al. 2015. High-spin Mn–oxo complexes and their relevance to the oxygen-evolving complex within photosystem II. *PNAS* 112:5319–24

69. Taguchi T, Gupta R, Lassalle-Kaiser B, Boyce DW, Yachandra VK, et al. 2012. Preparation and properties of a monomeric high-spin Mn^V–oxo complex. *J. Am. Chem. Soc.* 134:1996–99

70. Dau H, Haumann M. 2008. The manganese complex of photosystem II in its reaction cycle—basic framework and possible realization at the atomic level. *Coord. Chem. Rev.* 252:273–95

71. Dau H, Zaharieva I. 2009. Principles, efficiency, and blueprint character of solar-energy conversion in photosynthetic water oxidation. *Acc. Chem. Res.* 42:1861–70

72. McEvoy JP, Brudvig GW. 2006. Water-splitting chemistry of photosystem II. *Chem. Rev.* 106:4455–83

73. Warren JJ, Mayer JM. 2015. Moving protons and electrons in biomimetic systems. *Biochemistry* 54:1863–78

74. Hillier W, Wydrzynski T. 2008. ^{18}O-water exchange in photosystem II: substrate binding and intermediates of the water splitting cycle. *Coord. Chem. Rev.* 252:306–17

75. Hillier W, Wydrzynski T. 2001. Oxygen ligand exchange at metal sites—implications for the O_2 evolving mechanism of photosystem II. *Biochim. Biophys. Acta* 1503:197–209

76. Hillier W, Wydrzynski T. 2004. Substrate water interactions within the photosystem II oxygen evolving complex. *Phys. Chem. Chem. Phys.* 6:4882–89

77. Nilsson H, Krupnik T, Kargul J, Messinger J. 2014. Substrate water exchange in photosystem II core complexes of the extremophilic red alga *Cyanidioschyzon merolae*. *Biochim. Biophys. Acta* 1837:1257–62

78. Messinger J, Badger M, Wydrzynski T. 1995. Detection of one slowly exchanging substrate water molecule in the S_3 state of photosystem II. *PNAS* 92:3209–13

79. Pérez Navarro M, Ames WM, Nilsson H, Lohmiller T, Pantazis DA, et al. 2013. Ammonia binding to the oxygen-evolving complex of photosystem II identifies the solvent-exchangeable oxygen bridge (μ-oxo) of the manganese tetramer. *PNAS* 110:15561–66

80. Siegbahn PEM. 2013. Substrate water exchange for the oxygen evolving complex in PSII in the S_1, S_2, and S_3 states. *J. Am. Chem. Soc.* 135:9442–49

81. Vinyard DJ, Khan S, Brudvig GW. 2015. Photosynthetic water oxidation: binding and activation of substrate waters for O–O bond formation. *Faraday Discuss.* 185:37–50

82. Tagore R, Chen H, Crabtree RH, Brudvig GW. 2006. Determination of μ-oxo exchange rates in di-μ-oxo dimanganese complexes by electrospray ionization mass spectrometry. *J. Am. Chem. Soc.* 128:9457–65

83. Tagore R, Crabtree RH, Brudvig GW. 2007. Distinct mechanisms of bridging-oxo exchange in di-μ-O dimanganese complexes with and without water-binding sites: implications for water binding in the O_2-evolving complex of photosystem II. *Inorg. Chem.* 46:2193–203

84. Rotzinger FP. 1997. Mechanism of water exchange for the di- and trivalent metal hexaaqua ions of the first transition series. *J. Am. Chem. Soc.* 119:5230–38

85. Richens DT. 1997. *The Chemistry of Aqua Ions*. Chichester, UK: Wiley

86. Noguchi T, Suzuki H, Tsuno M, Sugiura M, Kato C. 2012. Time-resolved infrared detection of the proton and protein dynamics during photosynthetic oxygen evolution. *Biochemistry* 51:3205–14

87. Rappaport F, Blanchard-Desce M, Lavergne J. 1994. Kinetics of electron transfer and electrochromic change during the redox transitions of the photosynthetic oxygen-evolving complex. *Biochim. Biophys. Acta* 1184:178–92

88. Razeghifard MR, Pace RJ. 1997. Electron paramagnetic resonance kinetic studies of the S states in spinach PSII membranes. *Biochim. Biophys. Acta* 1322:141–50

89. Sugiura M, Kato Y, Takahashi R, Suzuki H, Watanabe T, et al. 2010. Energetics in photosystem II from *Thermosynechococcus elongatus* with a D1 protein encoded by either the *psbA1* or *psbA3* gene. *Biochim. Biophys. Acta* 1797:1491–99

90. Sugiura M, Inoue Y. 1999. Highly purified thermo-stable oxygen-evolving photosystem II core complex from the thermophilic cyanobacterium *Synechococcus elongatus* having His-tagged CP43. *Plant Cell Physiol.* 40:1219–31

91. Ananyev G, Dismukes GC. 2005. How fast can photosystem II split water? Kinetic performance at high and low frequencies. *Photosynth. Res.* 84:355–65

92. de Wijn R, van Gorkom HJ. 2001. Kinetics of electron transfer from Q_A to Q_B in photosystem II. *Biochemistry* 40:11912–22

93. Robinson HH, Crofts AR. 1983. Kinetics of the oxidation-reduction reactions of the photosystem II quinone acceptor complex, and the pathway for deactivation. *FEBS Lett.* 153:221–26

94. Weiss W, Renger G. 1984. UV-spectral characterization in Tris-washed chloroplasts of the redox component D1 which functionally connects the reaction center with the water-oxidizing enzyme system Y in photosynthesis. *FEBS Lett.* 169:219–23

95. Cao J, Govindjee. 1990. Chlorophyll *a* fluorescence transient as an indicator of active and inactive photosystem II in thylakoid membranes. *Biochim. Biophys. Acta* 1015:180–88

96. Schatz GH, Brock H, Holzwarth AR. 1988. Kinetic and energetic model for the primary processes in photosystem II. *Biophys. J.* 54:397–405

97. Kato Y, Nagao R, Noguchi T. 2016. Redox potential of the terminal quinone electron acceptor Q_B in photosystem II reveals the mechanism of electron transfer regulation. *PNAS* 113:620–25

98. Bard AJ, Faulkner LR. 2001. *Electrochemical Methods: Fundamentals and Applications*. New York: Wiley

99. Petersen J, Förster K, Turina P, Gräber P. 2012. Comparison of the H^+/ATP ratios of the H^+-ATP synthases from yeast and from chloroplast. *PNAS* 109:11150–55

100. Rosing J, Slater EC. 1972. The value of $\Delta G°$ for the hydrolysis of ATP. *Biochim. Biophys. Acta* 267:275–90

83. This is a careful experimental study of the chemical mechanism of μ-oxo exchange with bulk water in a Mn dimer complex.